Lipid imaging for visualizing cilastatin amelioration of cisplatin-induced nephrotoxicity

Estefanía Moreno-Gordaliza,[1,*] Diego Esteban-Fernández,[2,†] Alberto Lázaro,[2,§,] Sarah Aboulmagd,[†] Blanca Humanes,[§] Alberto Tejedor,[§,††] Michael W. Linscheid,[†] and M. Milagros Gómez-Gómez***

Department of Analytical Chemistry, Faculty of Chemistry,* and Department of Physiology,** and Department of Medicine,[††] School of Medicine, Universidad Complutense de Madrid, 28040 Madrid, Spain; Department of Chemistry,[†] Humboldt Universität zu Berlin, 12489 Berlin, Germany; and Renal Pathophysiology Laboratory, Department of Nephrology,[§] Instituto de Investigación Sanitaria Gregorio Marañón, Hospital General Universitario Gregorio Marañón, 28007 Madrid, Spain

ORCID IDs: 0000-0003-0606-3056 (E.M.); 0000-0001-9530-4194 (D.E.); 0000-0002-9904-4681 (M.M.G.)

Abstract **Nephrotoxicity is a major limitation to cisplatin antitumor therapies. Cilastatin, an inhibitor of renal dehydropeptidase-I, was recently proposed as a promising nephroprotector against cisplatin toxicity, preventing apoptotic cell death. In this work, cilastatin nephroprotection was further investigated in a rat model, with a focus on its effect on 76 renal lipids altered by cisplatin, including 13 new cisplatin-altered mitochondrial cardiolipin species. Lipid imaging was performed with MALDI mass spectrometry imaging (MALDI-MSI) in kidney sections from treated rats. Cilastatin was proved to significantly diminish the lipid distribution alterations caused by cisplatin, lipid levels being almost completely recovered to those of control samples. The extent of recovery of cisplatin-altered lipids by cilastatin turned out to be relevant for discriminating direct or secondary lipid alterations driven by cisplatin. Lipid peroxidation induced by cisplatin was also shown to be reduced when cilastatin was administered. Importantly, significant groups separation was achieved during multivariate analysis of cortex and outer-medullary lipids, indicating that damaged kidney can be discerned from the nephroprotected and healthy groups and classified according to lipid distribution. Therefore, we propose MALDI-MSI as a powerful potential tool offering multimolecule detection possibilities to visualize and evaluate nephrotoxicity and nephroprotection based on lipid analysis.**—Moreno-Gordaliza, E., D. Esteban-Fernández, A. Lázaro, S. Aboulmagd, B. Humanes, A. Tejedor, M. W. Linscheid, and M. M. Gómez-Gómez. **Lipid imaging for visualizing cilastatin amelioration of cisplatin-induced nephrotoxicity. *J. Lipid Res.* 2018.** 59: **1561–1574.**

Supplementary key words mass spectrometry • kidney • cancer • renal disease • molecular imaging • nephroprotection

Cisplatin has been successfully used in combinational therapies for the treatment of numerous solid tumors, with spectacular cure rates (higher than 90%) for testicular cancer (1). The drug is able to be hydrolyzed in cellular media and interact with DNA nucleobases, causing nuclear (2) (for proliferative cells) and mitochondrial damage, and leading to apoptotic cell death, where oxidative stress (OS) and inflammation are also involved (3, 4). In addition, interaction with other biomolecules, including proteins (5) or lipids (6), might contribute to the cytotoxic effect (7). Unfortunately, side effects such as nephrotoxicity can take place, with around 30% of the patients developing acute kidney injury (8), being the most limiting side effect to the drug administrable dose (1). Cisplatin particularly accumulates in the S3 segment of the proximal tubule (9), leading to cell death and renal dysfunction. In such nonproliferative cells, OS [involving reactive oxygen species

This work was supported by Minesterio de Economía y Competitividad Grants CTQ-2014-55711-R, CTQ2017-85673-R, ISCIII-FIS PI14/01195, and ISCIII-FIS PI17/00276, cofinanced by Federación Española de Enfermedades Raras funds from the European Commission "A Way of Making Europe"; Instituto de Salud Carlos III-RETIC REDinREN/RD16/0009/0026 and Comunidad de Madrid B2017/BMD-3686 (CIFRA2-CM). A.L. and A.T. are coinventors of patents describing cilastatin as a nephroprotector against toxic injuries that are assigned to Fundación para la Investigación Biomédica Hospital Gregorio Marañón and licensed to Spherium Biomed S.L.

Manuscript received 11 September 2017 and in revised form 12 July 2018.

Published, JLR Papers in Press, July 26, 2018
DOI https://doi.org/10.1194/jlr.M080465

Abbreviations: 4-HNE, 4-hydroxy-2-nonenal; 9-AA, 9-aminoacrydine; AA, arachidonic acid; bw, body weight; BUN, blood urea nitrogen; CL, cardiolipin; DHB, 2,5-dihydroxybenzoic acid, DHP-I, renal dehydropeptidase-I; FDR, false discovery rate; GFR, glomerular filtration rate; HE, hematoxylin & eosin; KIM-1, Kidney Injury Molecule-1; LPC, lysophosphatidylcholine; LPE, lysophosphatidylethanolamine; LPG, lysophosphatidylglycerol; LPI, lysophosphatidylinositol; LPS, lysophosphatidylserine; MSI, mass spectrometry imaging; OS, oxidative stress; PA, phosphatidic acid; PC, phosphatidylcholine; PCA, principal component analysis; PE, phosphatidylethanolamine; PG, phosphatidylglycerol; PI, phosphatidylinositol; PLA2, phospholipase A2; PLS-DA, partial least squares discriminant analysis; PS, phosphatidylserine; ROI, region of interest; RPTEC, renal proximal tubule epithelial cell; TFA, trifluoroacetic acid; VIP, variance in projection.

[1] To whom correspondence should be addressed.
e-mail: emorenog@ucm.es
[2] D. Esteban-Fernández and A. Lázaro contributed equally to this work.

[S] The online version of this article (available at http://www.jlr.org) contains a supplement.

generation and consequent damage of lipids, proteins, or DNA (10)], nitrosative stress, and mitochondrial damage are particularly involved, with extrinsic and intrinsic apoptotic pathways taking place (3).

Numerous nephroprotective approaches based on different molecular targets have been tested in vivo and in vitro for cisplatin (1, 11). However, nephroprotection is often incomplete, and the possible effect on the cytotoxicity of tumor cells is usually unclear (1). Cilastatin, a selective inhibitor of renal dehydropeptidase-I (DHP-I), has been shown to act as an effective nephroprotector for cisplatin in in vitro (12) and in vivo (9, 10) models without affecting the antitumor effect of the drug. Its ability to inhibit apoptosis and OS and to decrease inflammatory response in renal proximal tubule epithelial cells (RPTECs) has been demonstrated (10, 12–15), although the complete mechanism of nephroprotection of cilastatin is not completely understood.

Omics methodologies, including metallomics (16, 17), proteomics (18, 19), or metabolomics (20, 21) have shown a high potential for unraveling cisplatin mechanisms of toxicity (18), discovery of possible therapeutic targets for nephroprotection, and suggestion of new biomarkers of renal damage (22).

Aside from their structural roles, lipids can be involved in cell signaling and metabolism (23), but their levels can be altered as a consequence of pathological conditions. Lipid peroxidation in kidney is increased as a consequence of cisplatin-induced OS (24). In addition, triglyceride and NEFA levels were found to be raised in kidney extracts during cisplatin treatment (21). Phosphatidylcholine (PC) levels were also altered in lysates from human embryonic kidney cells treated with cisplatin (25), whereas differences have been reported in the membrane phospholipid composition of sensitive and resistant cells to cisplatin treatment (26). Other lipidomics studies have also suggested a connection of lipid abnormalities in plasma with chronic kidney disease (23) or diabetic nephropathy (27).

Direct mapping of intact biomolecules (28–31) on biological samples [e.g., 5–10 µm thick tissue sections or even cells (32, 33)] can be performed using MALDI mass spectrometry imaging (MALDI-MSI) (34). This technique provides high spatial resolutions (typically 10–50 µm) (30, 35) and offers unique molecular distribution information in tissue with quantitative possibilities (36). Previous works have demonstrated that different lipid distributions can be found in different renal compartments in the normal kidney (37, 38), which can be expected, considering the structural and functional differences found along the nephron. On the other hand, under certain nephropathies (39, 40) or during polycystic kidney disease (41), lipid alterations can be observed directly in tissue sections. Recent research also demonstrated that cisplatin treatment caused phospholipid distribution alterations in rat kidney sections, including PC, phosphatidylethanolamine (PE), phosphatidylserine (PS), phosphatidylglycerol (PG), phosphatidylinositol (PI), phosphatidic acid (PA), or lysophospholipids (LPLs) (42). Therefore, this suggests MALDI-MSI as a potentially useful tool for identifying renal damage beyond traditional methods.

Herein, we have further investigated the nephroprotective effect of cilastatin in a cisplatin-treated rat model, with a special focus in kidney lipid distribution. Moreover, we have explored the possibility of using MALDI-MSI as an alternative tool for nephroprotection and nephrotoxicity evaluation in kidney sections with promising results.

MATERIALS AND METHODS

Chemicals

Cisplatin was obtained from Pharmacia Nostrum (Madrid, Spain). Cilastatin was kindly offered by Merck Sharp and Dohme S.A. (Madrid, Spain). Both drugs were dissolved in 0.9% NaCl solution (Braun Medical S.A, Barcelona, Spain) for administration. The 2,5-dihydroxybenzoic acid (DHB) and 9-aminoacrydine (9-AA), used as MALDI matrices, and methanol (MeOH), acetonitrile (ACN), 2-propanol (iPrOH), and trifluoroacetic acid (TFA), used as matrix solvents, were all purchased from Sigma-Aldrich (Steinheim, Germany).

Animals and tissue sections

Female, 7 week old Wistar rats (WKY, Criffa, Barcelona, Spain) were treated at the animal facilities of the Instituto de Investigación Sanitaria Gregorio Marañón (IiSGM, Madrid, Spain). The animals were fed and provided water ad libitum and kept under controlled light (12 h light/dark cycle), temperature, and humidity conditions. All the procedures were approved by the Ethics Committee on Animal Experimentation from the IiSGM, and animals were treated in accordance with Directive 2010/63/EU and of Spanish Royal Decree 53/2013 on the protection of animals used for experimentation and other scientific purposes.

Four groups of rats were administered treatments by intraperitoneal injection (i.p.) as previously described (9, 10): *1*) control rats injected a 0.9% NaCl solution in the same doses and regimes of groups 3 and 4 (n = 4); *2*) cilastatin-treated rats [150 $mg \cdot kg^{-1}$ of body weight (bw) per day, n = 4]; *3*) cisplatin-treated rats (single dose of 5 $mg \cdot kg^{-1}$ bw at day 0, i.p., n = 4); and *4*) cisplatin (as in group 3) plus cilastatin (as in group 2) treated rats (n = 4). After 5 days of treatment, animals were anesthetized and euthanized. Prior to the euthanization, urine from each animal was collected for 24 h in metabolic cages. Serum was obtained by centrifugation of blood samples. Kidneys were perfused with saline solution at 4°C, removed, decapsulated, and wrapped in aluminum foil, followed by snap-freezing in liquid N_2 and stored at −80°C. Sagittal sections of 5 or 10 µm thickness were obtained with a cryostat (Thermo Fisher Scientific, model no. HM525 NX) at −20°C, thaw-mounted onto Superfrost Plus slides (Thermo Fisher Scientific, Braunschweig, Germany), and stored at −80°C.

Histological studies

The 5 µm sagittal rat kidney sections were stained with hematoxylin–eosin (HE) (Sigma-Aldrich). Microphotographs were taken from the sections for histological examination using an inverted IX70 microscope (Olympus, Hamburg, Germany) with 20× and 60× magnification.

Renal failure-indicating biochemical parameters

Blood urea nitrogen (BUN) and creatinine were determined in serum using a modular AutoAnalyzer Cobas 711 (Roche, Basel, Switzerland). Glomerular filtration rate (GFR) was calculated by

using creatinine clearance rate. The sulfosalicylic acid method (43) was used for total protein analysis in urine.

Immunohistochemistry

Immunohistochemistry was carried out on 5 μm tissue sections as previously described (10). Polyclonal anti-Kidney Injury Molecule-1 (anti-KIM-1) (R&D Systems; dilution 1:20) and monoclonal anti-4-hydroxy-2-nonenal (anti-4-HNE) (Oxis International Inc., Foster City, CA; dilution 1:75) were used as primary antibodies. The specificity of the antibodies was verified by controls lacking the primary antibody, producing no background. The surface area labeled by the antibodies was evaluated by quantitative image analysis (10).

Apoptosis detection

DNA fragmentation, an apoptosis indicator, was determined by TUNEL assay in 5 μm kidney tissue sections using a Fluorescein FragEL DNA Fragmentation Detection Kit (Calbiochem, San Diego, CA), as previously described (10). A confocal microscope (Leica-SP2, Leica Microsystems, Heidelberg, Germany) was employed for visualization of TUNEL-positive cells. For each renal section, cells undergoing apoptosis were quantified in a blinded manner by counting all positive apoptotic cells in eight nonoverlapping random fields viewed at 20× magnification.

MALDI-MSI

First, 10 μm kidney slices were thawed inside a desiccator. Either DHB (60 mg·ml^{-1} in 70% MeOH with 0.1% TFA) or 9-AA (60 mg·ml^{-1} in 70% iPrOH/ACN (60:40) with 0.1% TFA) were used as matrices for positive or negative ion mode analysis, respectively. Each matrix was applied on the tissues with an airbrush in 15 cycles comprising deposition for 20 s followed by drying for 40 s, as previously described (42).

Data were acquired using a MALDI LTQ Orbitrap XL Pro mass spectrometer (Thermo Scientific, San José, CA), and laser intensity was adjusted to 22.5 μJ for DHB and 25–30 μJ for 9-AA. Imaging was performed in rastering mode, with a spatial resolution of 100 μm. Mass spectra were registered in full-scan mode at *m/z* 200–2,000 and 2 microscans per step either in positive or negative ion mode, with a 60,000 mass resolution on the Fourier Transform MS analyzer. Data processing was carried out using ImageQuest software (Thermo Scientific), MS images were extracted with 0.008 Da tolerance, and total ion current (TIC) normalization was applied. MSI raw files were converted to imzML (44) using ImageQuest and further processed with MSiReader (45) for tissue comparison in substructural renal features. Data were extracted from six regions of interest (ROIs) per treatment type and substructure, each ROI comprising 200 data points. For exact mass identification, a database search in LipidMaps (46) and LipidBlast (47) was performed with a mass tolerance of 5 ppm. Lipid identification was assisted with MS/MS fragmentation experiments carried out in the ion trap by collisionally induced dissociation at 35% energy.

Statistical analysis

Quantitative variables were expressed as mean ± SEM. SPSS (Version 11.5; SPSS, Chicago, IL) was used for descriptive statistics and evaluating statistical differences in variables between groups by ANOVA. Lipid variables from ROIs were compared between groups using Mann–Whitney and Kruskal–Wallis tests with SPSS 11.5. A significance level of 0.05 was employed for identifying statistically significant differences. False discovery rate (FDR) correction was performed using the Benjamini–Hochberg method. Multivariate analysis, including principal component analysis (PCA) and partial least squares discriminant analysis (PLS-DA), was performed using MetaboAnalyst (Version 3.0) (48). Lipid data extracted from MSiReader (45) were TIC-normalized, log-transformed, and pareto-scaled prior to multivariate analysis.

Lipid nomenclature

The nomenclature for lipids proposed by the LipidMaps consortium (46) was employed. Briefly, glycerophospholipids [PE, PC, PS, PI, PI phosphate (PIP), phosphatidyl inositol ceramide (PI-Cer), PG, lysophosphatidylethanolamine (LPE), lysophosphatidylcholine (LPC), lysophosphatidylserine (LPS), lysophosphatidylinositol (LPI), lysophosphatidylglycerol (LPG), PA, and cardiolipins (CLs)] are designated followed by (W:X), W being the total acyl chains length and X the total amount of double bonds. Sphingolipids (SM and sulfatides, including SM2a and SM4s-), are followed by (Y:Z), where Y is the length of the sphingosine-bound acyl chain and Z is the total amount of double bonds in the chain. Alkyl ether linkage and (1Z)-alkenyl ether, are designated by "O-" and "P-", respectively. Finally, "h", "d," and "t" indicate 1-hydroxy, 1,3 dihydroxy, and 1,3,4-trihydroxy, respectively, sphingolipid long-chain bases.

RESULTS

Cilastatin attenuation of cisplatin-induced bw loss

Supplemental Table S1 shows how cisplatin treatment leads to a significant increase in rat bw loss compared with control rats. Importantly, cilastatin cotreatment with cisplatin partially attenuated the effect exerted by the latter. Cilastatin alone did not have any impact on rat bw with respect to control animals.

Cilastatin effect on classical indicators of cisplatin-induced renal injury

Renal function in treated animals was assessed with classical biochemical indicators. Serum creatinine, BUN, urinary volume, and urinary proteins (all of them significantly increased during cisplatin treatment with respect to control animals) were decreased to control levels in the presence of cilastatin, as shown in **Table 1**. GFR was decreased during cisplatin treatment with respect to control samples, confirming renal damage, whereas cotreatment with cilastatin prevented this effect. On the other hand, treatment with only cilastatin did not affect any of the above parameters.

Cilastatin protects against cisplatin-induced morphological renal lesions

Histology was examined in HE-stained sections in search of morphological alterations related to renal damage. **Figure 1** shows a normal morphology in control and cilastatin-treated renal sections. However, cisplatin treatment displayed clear signs of nephrotoxicity in the proximal renal tubules, including tubule swelling, cell debris detachment, hyaline casts accumulation, or loss of brush border membrane (Fig. 1C, E, G), all of them being significantly prevented with the use of cilastatin (Fig. 1, F, H).

Cilastatin decreases expression of cisplatin-induced early renal damage markers

KIM-1 has been described as a protein biomarker of early renal damage measurable in tissue and urine (49).

TABLE 1. Protective effect of cilastatin of renal function under cisplatin treatment

Groups	S_{Creat} (mg/dl)	BUN (mg/dl)	GFR (ml/min/100 g)	U_{Vol} (ml/24 h)	U_{Prot} (mg/24 h)
Control	0.44 ± 0.01	16.9 ± 0.9	0.46 ± 0.06	7 ± 2	1.4 ± 0.6
Control + cilastatin	0.42 ± 0.07	17 ± 1	0.52 ± 0.08	10 ± 1	1.65 ± 0.07
Cisplatin	3 ± 1[a]	100 ± 30[a]	0.16 ± 0.06[a]	24 ± 2[a]	6 ± 1[b]
Cisplatin+ cilastatin	0.6 ± 0.1	14 ± 2	0.40 ± 0.04	10 ± 1	1.6 ± 0.3

Results are expressed as mean ± SEM. S_{Creat}, serum creatinine; U_{Prot}, urinary protein; U_{Vol}, urinary volume.
[a] $P < 0.05$ versus other groups (in each column).
[b] $P < 0.005$ versus other groups (in this column).

KIM-1 expression was measured in kidney sections by immunostaining, as shown in Fig. 1. KIM-1 was significantly overexpressed in proximal tubule cells, mainly in the corticomedullary junction, renal cortex, and outer medulla of the cisplatin-treated group (Fig. 1K, M), in comparison with the control group (Fig. 1I). This was significantly ameliorated when cilastatin was coadministered with cisplatin (Fig. 1L, N), whereas cilastatin alone (Fig. 1J) did not have any effect on KIM-1 expression compared with the control tissue (Fig. 1I).

Cilastatin attenuates cisplatin-induced apoptosis

Apoptosis was evaluated by TUNEL in kidney sections, as shown in supplemental Fig. S1. Cisplatin turned out to increase the number of TUNEL-positive cells (supplemental Fig. S1C) with respect to control samples (supplemental Fig. S1A), as quantified in supplemental Fig. S1E. Treatment with cilastatin significantly decreased the number of TUNEL-positive cells when coadministered with cisplatin (supplemental Fig. S1D), whereas cilastatin itself (supplemental Fig. S1B) did not exert any relevant effect compared with control kidney, as can be seen in supplemental Fig. S1E.

Cilastatin reduces lipid peroxidation associated to cisplatin treatment

The 4-HNE is a product of FA oxidation and is considered an OS biomarker (50). Lipid peroxidation was determined by 4-HNE immunohistochemical detection in kidney sections. Cisplatin treatment resulted in increased 4-HNE staining in kidney (supplemental Fig. S2C) with respect to control tissue (supplemental Fig. S2A). Again, cotreatment with cilastatin prevented cisplatin-induced increase of 4-HNE (supplemental Fig. S2D), whereas cilastatin alone did not modify 4-HNE production (supplemental Fig. S2B) compared with the control tissue, as shown in supplemental Fig. S2E.

Cilastatin diminishes cisplatin-induced alterations of renal lipids

The distribution of certain renal lipids was previously found to be altered under treatment with cisplatin in a rat model (42). In order to evaluate the countereffect of cilastatin on cisplatin-induced lipid alterations, images for lipids were produced in positive and negative mode by MALDI-MSI in kidney sections from rats either untreated or treated with cisplatin, cilastatin, or the combination of the latter two. **Figure 2** summarizes the effect of cisplatin treatment on the renal distribution of 76 lipid species (including 13 newly found CLs decreased by cisplatin) and uridine diphosphate *N*-acetylglucosamine (UDP-GlcNAc), along with the protective effect of cilastatin. Supplemental Table S2 presents the complete renal lipid distribution for the four groups of samples analyzed with both ionization modes, along with lipid identification data. Additionally, **Fig. 3** shows images for selected structural lipids detected in positive mode, including PC(34:2), PE(38:7), PC(34:0), PC(36:5), and PC(40:6) species, whereas **Fig. 4** shows images for negative mode-detected lipids, including PA(36:4), LPI(18:0), PI(38:4), PS(36:4), PI(36:2) CL(72:8), PG(34:1), or SM4 (t18:0, h24:1). The HE-stained parallel slices and the local lipid intensities found in the cortex and outer medulla for the four types of samples are also displayed in Figs. 3 and 4. As shown in supplemental Table S2, and illustrated in Figs. 2–4, in contrast to the cisplatin-induced effect observed, coadministration of cilastatin along with cisplatin attenuated these lipid alterations either totally (for 31 species, where lipid distributions were comparable to those of control kidney samples) or partially (for 39 lipid species). Only in the case of seven lipid species [PI(40:7), SM4(t18:0, h24:1), CL(70:6), CL(70:7), CL(70:8), CL(70:9), and CL(72:10)], no significant differences in renal distribution were observed between cisplatin and cisplatin+cilastatin-treated groups, and therefore no recovery was observed. On the other hand, treatment with cilastatin alone led to no relevant changes in the main renal lipid distribution in comparison to control samples, as shown in Figs. 3 and 4 and supplemental Table S2.

Figure 5 shows a lipid class-based analysis of the effects of cisplatin on renal lipids. PI and PC are the main lipid classes increasing in renal cortex due to cisplatin treatment, followed by LPG, PG, and PS (Fig. 5A). Furthermore, PC is the main lipid type displaced from cortex to medulla after cisplatin treatment (Fig. 5B), whereas PI, LPG, LPI, PS, and PG are the main lipids that are simultaneously increased in cortex and medulla during cisplatin treatment (Fig. 5C). Moreover, Fig. 5D, E shows the effect of cisplatin on the amount of double bonds found in renal cortex lipids, with the overall trend to reduce the degree of PUFA-containing phospholipids. Finally, Fig. 5F, G displays the effect of cilastatin on cisplatin-induced changes on cortex and medulla lipids, according to their class type, showing a tendency of recovery of control lipid distribution for most of the lipid classes.

Discrimination of cisplatin-treated and cilastatin-protected kidney based on multivariate analysis of cortical and medullary lipids

PCA performed on cortex and outer medulla lipids found in positive (**Fig. 6B**, D) and negative ionization mode

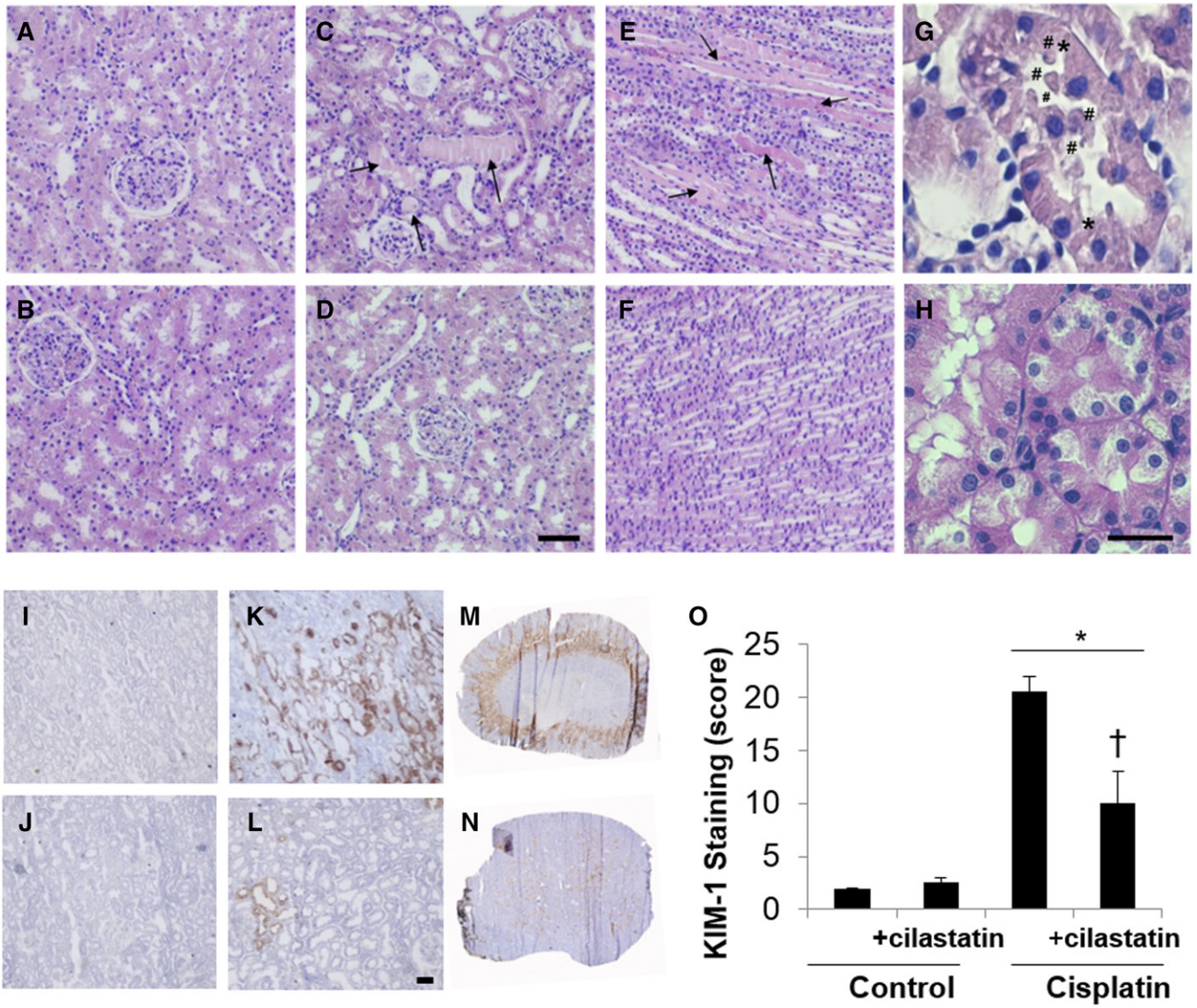

Fig. 1. Cilastatin prevents cisplatin-induced morphological lesions and reduces the expression of the early renal damage marker KIM-1. The 20× microscope images for HE-stained kidney sections for control (cortex) (A), control+cilastatin (cortex) (B), cisplatin (cortex, C; and medulla, E), cisplatin + cilastatin (cortex, D; and medulla, F). The 60× magnified images are displayed in for cortex areas in cisplatin (G) and cisplatin+cilastatin (H). Cisplatin-induced signs of damage are depicted as follows: hyaline casts are indicated with arrows; # denotes cell debris detachment; and * represents loss of intercellular junctions. D, H: Scale bars represent 100 (D) or 25 (H) μm. Microscopy images for immunostained kidney sections for KIM-1 detection visualized at 20× are compared for control (I), control + cilastatin (J), cisplatin (K), and cilastatin + cisplatin (L). Whole kidney images for cisplatin-treated (M) and cilastatin + cisplatin-treated (N) rats. L: Scale bar represents 50 μm size. O: Quantitative results for KIM-1 staining are expressed as mean ± SEM; n = 4 animals per group. * $P < 0.05$ versus control and control+cilastatin groups; † $P < 0.02$ versus cisplatin group.

(Fig. 6A, C) led to a clear group separation of cisplatin-treated kidney with respect to control, cilastatin-treated, and cisplatin+cilastatin-treated groups, the latter resembling more control groups. PLS-DA led to analogous group discrimination for cortex and outer medulla lipids, as shown in supplemental Figs. S3 and S4, respectively. As can be seen, the group treated both with cisplatin and cilastatin tended to completely separate from the rest of the groups in the PLS-DA. Variance in projection (VIP) scores for PLS-DA of the four groups are also presented in supplemental Figs. S3 and S4 for cortex and medulla lipids, respectively, indicating relevant features leading to groups separation with a 1.0 cut-off. Good prediction models were obtained for all cases, with R^2 and Q^2 higher than 0.9, considering three components.

Separate PLS-DA of cisplatin versus control groups are presented for lipids in positive (Fig. 6E, F) and negative (supplemental Fig. S5A, B) ionization modes for cortex and medulla, respectively. According to the corresponding VIP scores (Fig. 6G, H; supplemental Fig. S5C, D), PC(42:10), PC(36:3), PC(40:7), PC(34:2), and PI(38:4) in cortex and PG(37:7), PC(38:4), PE(38:7), PC(38:4), PC(40:6), PE(36:4), and LPC(18:0) in medulla are the positive lipids contributing the most to cisplatin discrimination with respect to the control group. In negative mode, PI-Cer(t44:0), PI(39:4), PG(34:1), PS(40:7), LPG(20:5), and

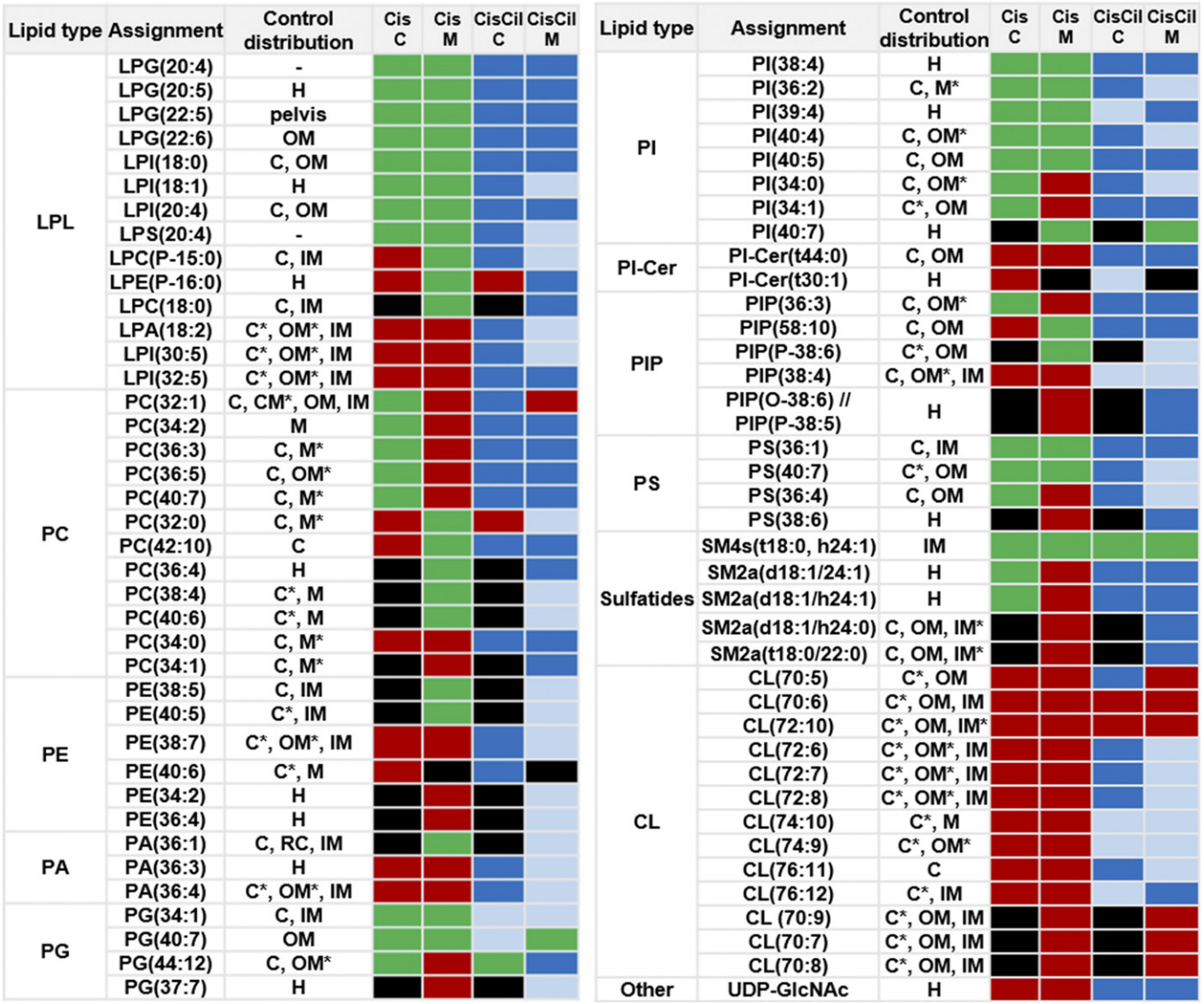

Fig. 2. Protective effect of cilastatin against cisplatin-induced alterations on cortical and medullary renal lipids. MALDI-MSI relative quantification results are shown for 77 species (76 lipids), according to their lipid class, for control rat kidney versus cisplatin (Cis) or cisplatin+cilastatin (CisCil)-treated kidney in cortex (C) and medulla (M). The effect of cisplatin and cilastatin with respect to control lipid levels (with FDR < 0.05) is presented with the following color code: red, decrease versus control; green, increase versus control; black, no change versus control; blue, total recovery versus control levels; light blue, partial recovery versus control levels. Control kidneys lipid location is presented with the following abbreviations: C, cortex; CM, corticomedullary junction; H, homogeneous distribution; IM, inner medulla; M, medulla (including OM and IM); OM, outer medulla; RC, renal column. * denotes kidney region with the highest lipid intensity, when present in several regions.

PI(38:4) in cortex and LPS(20:4), LPG(22:5), LPG(20:4), LPG(20:5), PIP(36:3), and CL(78:5) in medulla are the variables contributing the most to discriminating cisplatin from control groups.

MALDI imaging of lipids allows visualizing nephrotoxicity and nephroprotection effects

MALDI-MSI allows simultaneous acquisition of data for building distribution images for hundreds of lipid species in a tissue section. Combining information on multiple species could lead to a more reliable assessment of renal damage or nephroprotection in tissue. **Figure 7** shows individual renal distributions for $[M\text{-}H]^-$ ions for PA(36:1) at m/z 701.5145 and PI(34:0) at m/z 837.5529, along with merged images for both species for the four types of animal groups. Two clearly distinct patterns were observed for the samples either with no renal damage (control, Fig. 7A–C; cilastatin, Fig. 7D–F; and cilastatin coadministered with cisplatin, Fig. 7J–L) or presenting cisplatin-induced acute kidney injury (Fig. 7G–I). These differences were enhanced in the merged images for both lipids distribution.

DISCUSSION

Nephrotoxicity is a serious side effect of several therapies, including cisplatin (51). Cisplatin is able to accumulate in RPTECs, leading to OS, nuclear and mitochondrial

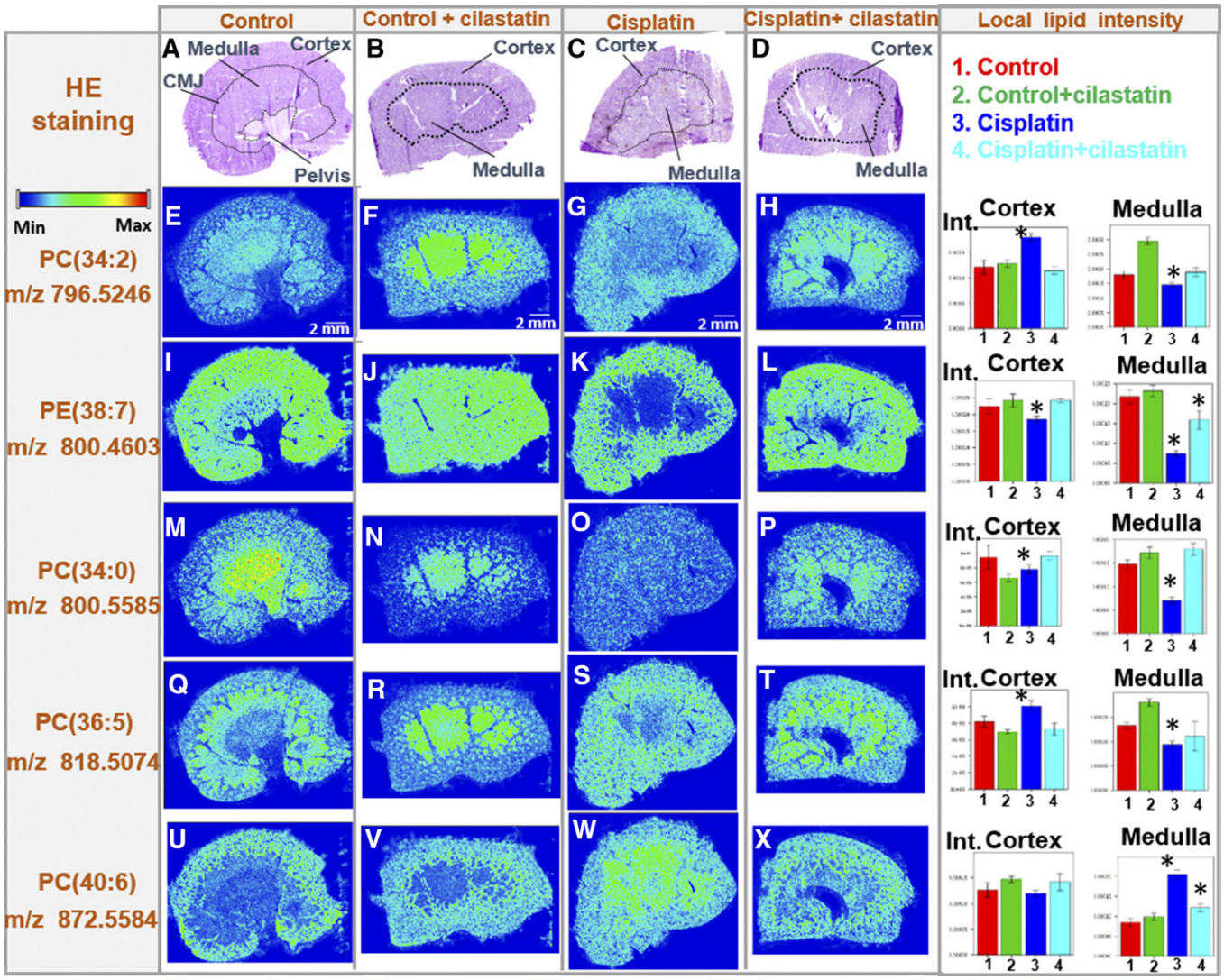

Fig. 3. Cilastatin protects against cisplatin-induced lipid alterations: structural lipids (PC and PE) found in positive ion mode. HE-stained kidney sections images are displayed (A–D for control, control+cilastatin, cisplatin, and cisplatin+cilastatin, respectively) along with the delimited cortex, medulla, and corticomedullary junction (CMJ) regions. Their respective MALDI-MSI images in positive-ion mode for selected lipid distributions have been included below each HE image: PC(34:2) (E–H), PE(38:7) (I–L), PC(34:0) (M–P), PC(36:5) (Q–T), and PC(40:6) (U–X). Color-scale bar is shown for lipid images. Right: Bar charts for the local lipid intensities observed for the four groups in either kidney cortex or medulla are displayed next to the lipid distribution images for each of the lipid species selected. Control (1), control+cilastatin (2), cisplatin (3), and cisplatin+cilastatin (4) groups are represented in red, green, blue, and cyan, respectively. * FDR < 0.05 versus all other groups; # FDR < 0.05 versus control group.

damage, apoptotic (and also necrotic) cell death, and renal failure (8). Cilastatin was recently shown to effectively protect against nephrotoxicity induced by cisplatin (10), vancomycin (13), cyclosporine A, and tacrolimus (52) and to enable restored renal function. As previously reported, cilastatin interacts with DHP-I located in the brush border lipid raft of RPTECs, thus inhibiting its enzymatic activity (53) and preventing any related transport or signaling based on vesicle internalization (13). Therefore, cilastatin can inhibit the extrinsic pathway of apoptosis and, to some extent, reduce luminal entry of drugs in DHP-I-bearing RPTECs without interfering with the pharmacological effect of cisplatin in target cells (12).

Consistent with our previous observations in a male rat model (10), we show that cilastatin protects against cisplatin-induced renal damage in a female rat model, ameliorating the effects of cisplatin on weight loss and renal function (measured in terms of GFR, serum creatinine, and BUN) and preventing renal lesions. In contrast to results from other studies (54), this finding confirmed the toxic effect of cisplatin and the protective effect of cilastatin, regardless of the animal's gender. The results of the TUNEL assay in tissue also supported this observation, with clearly diminished apoptotic cell death when cilastatin and cisplatin were coadministered, as compared with the tissues after treatment with cisplatin. Furthermore, KIM-1 staining in tissue made it possible to visualize and locate early renal damage caused by cisplatin in the renal cortex and outer medulla. This finding is in agreement with the fact that the S3 segment of the proximal tubule, the main focus of renal damage, is located in those same areas. Cotreatment of cisplatin with cilastatin revealed almost nondetectable

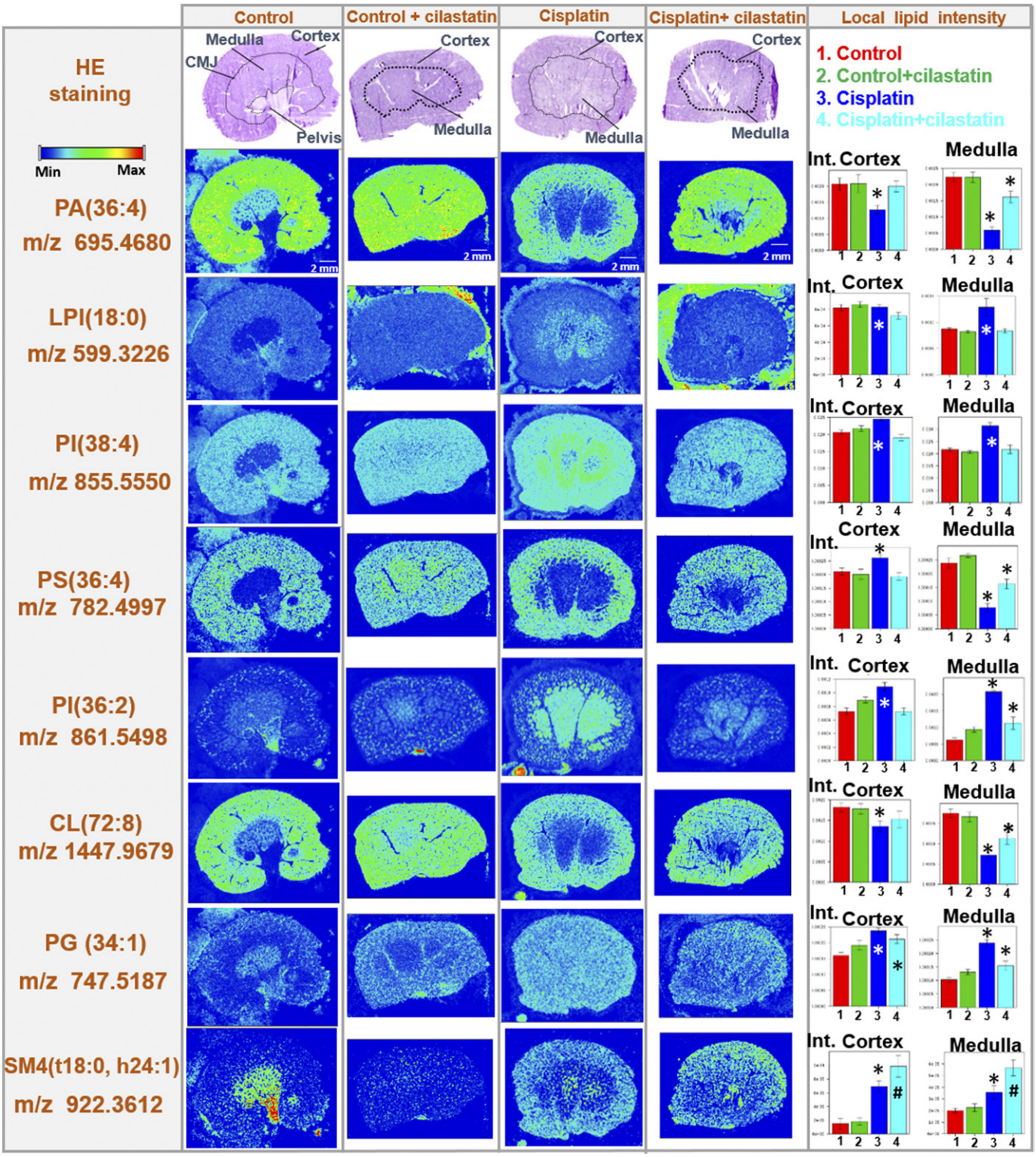

Fig. 4. Cilastatin protects against cisplatin-induced lipid alterations: lipids detected in negative ion mode. HE-stained kidney sections images are displayed (A–D for control, control+cilastatin, cisplatin, and cisplatin+cilastatin, respectively) along with the delimited cortex, medulla, and corticomedullary junction (CMJ) regions. Their respective MALDI-MSI images in negative-ion mode for selected lipid distributions have been included below each HE image: PA(36:4), LPI(18:0), PI(38:4), PS(36:4), PI(36:2), CL(72:8), PG(34:1), and SM4(t18:0, h24:1). Color-scale bar is shown for lipid images. Right: Bar charts for the local lipid intensities observed for the four groups in either kidney cortex or medulla are displayed next to the lipid distribution images for each of the lipid species selected. Control (1), control+cilastatin (2), cisplatin (3), and cisplatin+cilastatin (4) groups are represented in red, green, blue, and cyan, respectively. * FDR < 0.05 versus all other groups; # FDR < 0.05 versus control group.

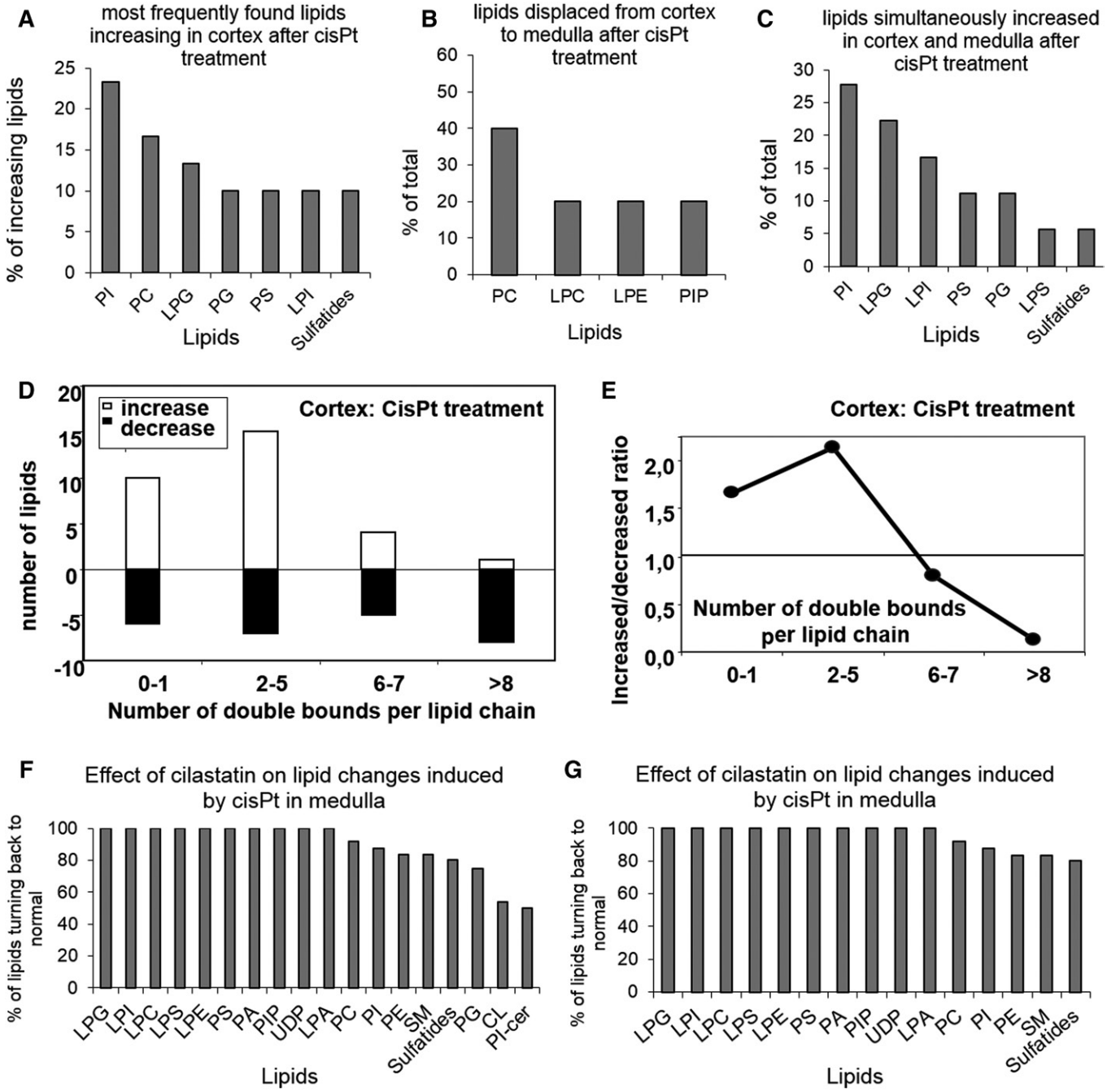

Fig. 5. Effect of cisplatin on renal lipids distribution, according to lipid class and number of acyl-chain double bonds, and the protective effect of cilastatin. Percentage of renal species according to lipid class showing an increase in cortex (A), a displacement from cortex to medulla (B), and a simultaneous increase in cortex and medulla (C) after cisplatin (cisPt) treatment. D: Percentage of lipids increasing (open bars) and decreasing (filled bars) in renal cortex after cisplatin treatment according to the amount of double bounds in the acyl chains. E: Ratio of increased versus decreased lipids in cortex after cisplatin treatment, according to the amount of double bounds in the acyl chains. The restoring effect of cilastatin against cisplatin-induced changes according to lipid class is displayed in F and G for cortex and medulla, respectively.

expression of KIM-1, providing additional evidence on the nephroprotective effect of cilastatin. Moreover, signs of lipid peroxidation due to OS (based on 4-HNE detection) during treatment with cisplatin were not visible under protection with cilastatin.

Aside from causing lipid peroxidation, cisplatin was reported to modify the renal distribution of lipid species in controls in a rat model (42) in regions of the kidney where damage takes place, suggesting a correlation between the nephrotoxic effect exerted by the drug and the lipid changes induced (42). In this case, we studied the effect of cilastatin in 76 renal lipid species and UDP-GlcNAc, all of which were altered with cisplatin. This finding adds to previous results (42) with new, additional 13 CL species. To our knowledge, this is the first time their effect has been visualized. Cilastatin fully

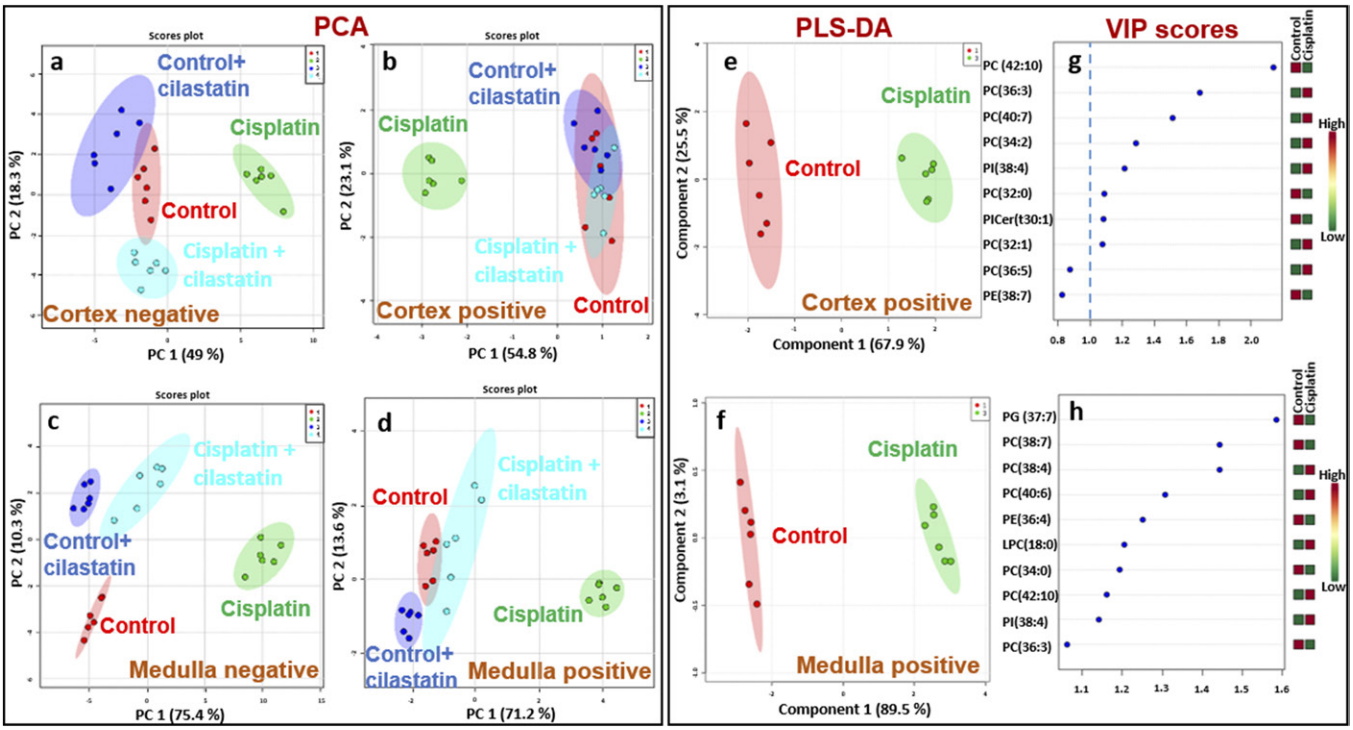

Fig. 6. Multivariate analysis shows that protected kidney (treated with both cilastatin and cisplatin) shares lipid features with control samples, separating from the cisplatin-treated group. PCA 2D score plots are shown for negative-ion mode lipids in cortex (A) and outer medulla (C) and positive-ion mode lipids in cortex (B) and outer medulla (D) for ROIs of the four groups of samples: control (red), control+cilastatin (green), cisplatin (green), and cisplatin+cilastatin (cyan). The 95% confidence areas are displayed for each group. PLS-DA 2D score plots are also shown for control (red) versus cisplatin (green) groups for cortex (E) and medulla (F) lipids detected in positive mode, along with the main lipid features ranked by VIP scores (G and H, respectively). A 1.0 cut-off for VIP scores is depicted in G and H.

or partially restored most of the cisplatin-altered lipid levels.

Among structural lipids, PC and, to a lesser extent, PE are the most abundant species in membranes (55). PC is the lipid type that best differentiates between control and cisplatin-treated kidney, especially PC(42:10) (Fig. 6), and the lipid class with the second highest increase in renal cortex in rats treated with cisplatin (Fig. 5A). Correlation with histology suggests that increased PC species in cortex might represent a regenerative cellular response after the initial cisplatin-induced damage. Moreover, cisplatin-induced proximal tubule cell damage leads to luminal release of apoptotic bodies with intact cell membranes, which can subsequently be trapped in the medulla by intratubular protein casts. This migration of fragments from damaged proximal tubule cells might explain why PC species are decreased in the cortex and increased in the medulla (Fig. 5B). Cilastatin, a specific ligand of proximal tubule cells that can block amplification of apoptosis, significantly restored most of the structural PC and PE lipids to control values in both the cortex and the medulla.

PI is the primary source of arachidonic acid [AA; FA(20:4)], which is released from the sn-2 position via the action of the enzyme phospholipase A2 (PLA2) (56, 57). The main PI species in kidney is PI(18:0/20:4), which belongs to the PI(38:4) family of isomers (55, 56, 58). In this case, several PI species were increased in either the cortex or the outer medulla after treatment with cisplatin. For instance, PI(38:4), the most abundant PI species in both the medulla and the cortex, was found to be increased after treatment with cisplatin in both substructures, especially in the outer medulla (Figs. 2 and 4). Cisplatin activates nuclear factor kappa β [thus triggering an increase in proinflammatory molecules and interleukins (15)], which can induce PLA2 (59). In addition, cisplatin is able to increase production of inflammatory species (15) during renal damage. Therefore, a subsequent increase in prostaglandins and thromboxanes, both of which are synthesized from AA, is to be expected in the outer medulla (the preferential area of AA synthesis) (60). Accordingly, a striking increase in LPI(18:0), a by-product of PLA2 activity on PI(18:0/20:4), is observed, especially in the outer medulla. Consistent with the observed increase in PI(38:4), these observations suggest an increase in turnover of AA for eicosanoid synthesis. However, a possible redistribution of arachidonate by acyl remodeling, as well as arachidonyl turnover, should not be ruled out. Therefore, cilastatin, which fully restores both PI(38:4) and LPI(18:0) and tends to restore other PI species too, is able to block cisplatin-induced apoptosis and its downstream effects. These results show, for the first time, the underlying process of our previous observations (10, 12, 15). Moreover, other phospholipids, such as PC, can also be a source of AA via PLA2. In addition, PC(36:4) [mainly PC(16:0/20:4) in kidney] (58), PC(38:4) [mainly PC(18:0/20:4) in kidney and the main renal PC species] (58), and LPC(18:0) are all exclusively increased in the outer medulla after treatment with cisplatin and practically restored to control values by

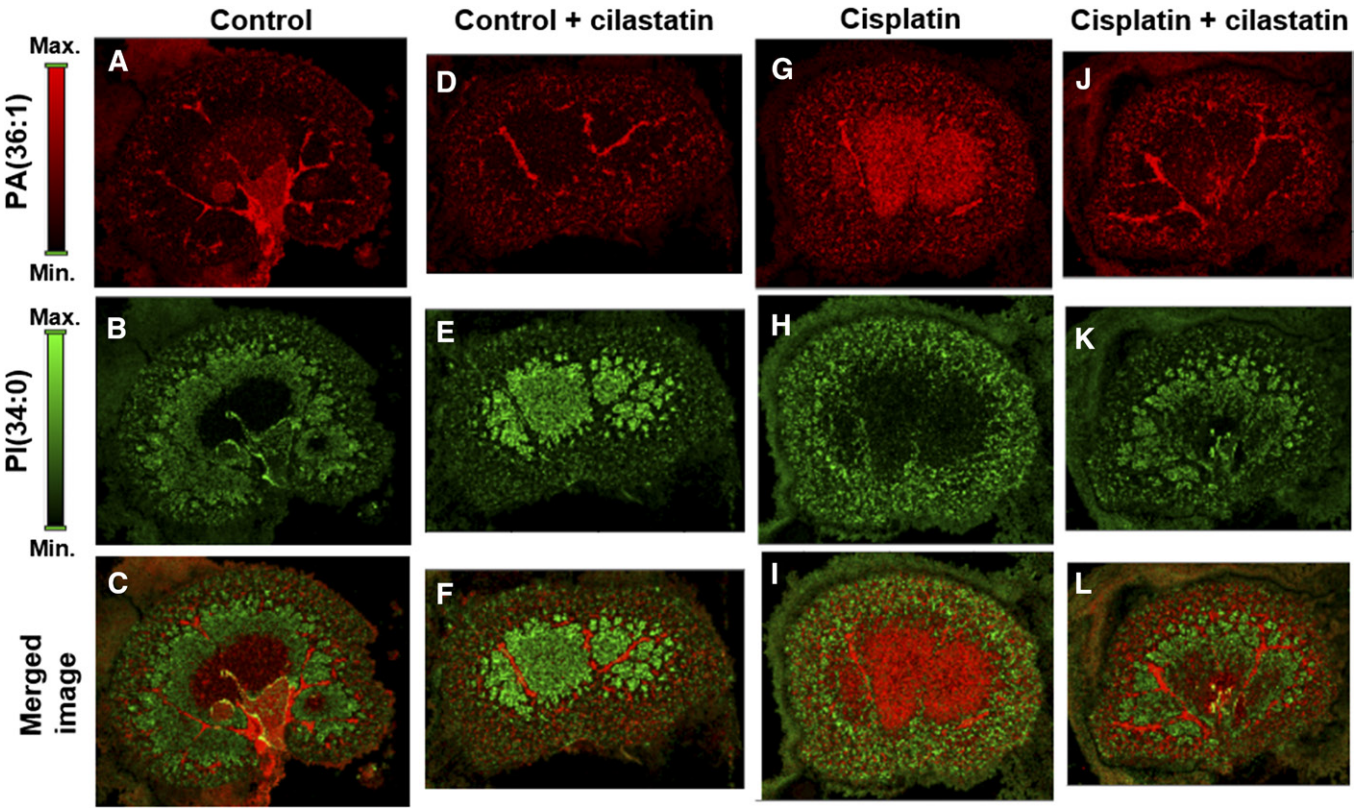

Fig. 7. Combined lipid species MALDI imaging for the assessment of renal damage and nephroprotection. MALDI-MSI images in negative-ion mode are presented for PA(36:1) at *m/z* 701.5145 (A, D, G, and J) and PI(34:0) at *m/z* 837.5529 (B, E, H, and K) and the merged image for both lipids (C, F, I, and L) for control, control+cilastatin, cisplatin, and cisplatin+cilastatin kidney slices, respectively. Color-scale bars are shown for both lipids.

cilastatin (Fig. 2). These findings point to the same metabolic activation as that described for PI(38:4).

A number of other LPL species, LPG, LPI, and LPS [cell signaling molecules (61)], were also found to be upregulated in the cortex and outer medulla during treatment with cisplatin. These proved to be highly discriminating variables for cisplatin-damaged kidney versus control tissue in PLS-DA. Furthermore, PS undergoes cell membrane externalization during apoptotic triggering (62) and induces PS-receptor-mediated scavenging of apoptotic cells (63). PS can be synthesized de novo from PE (64), thus explaining the cisplatin-induced increase in the cortex in several PS species (Fig. 2), which tends to return to control levels in the presence of cilastatin.

PG (mostly present in the mitochondrial membrane) is a precursor of CLs, which provide essential and functional support to proteins involved in mitochondrial respiration (65). CLs are found exclusively in mitochondrial membranes and can thus be considered a signature mitochondrial lipid class (65). A particularly high density of mitochondria can be found in the distal tubules (66), which are mainly located in the medulla. CL in the mitochondrial outer membrane provides an anchor for caspase-8, which translocates to mitochondria upon Fas receptor activation (67). Furthermore, peroxidation of CL seems to precede intrinsic apoptotic cell death (65). Accumulation of CL hydrolysis products, including AA, has been reported in vivo after acute tissue injury (68). Moreover, a decrease in CL has been reported in several cell types during apoptosis, prior to outer membrane permeabilization (69). According to our results, up to 13 CL species, including the most abundant CL in kidney, CL(72:8), followed by CL(72:7) and CL(74:10) (58, 70), proved to be decreased after treatment with cisplatin, mainly in the outer medulla, but also in the cortex for 10 of the CL species (Figs. 2 and 4). This finding is in agreement with the total cisplatin-induced decrease in CL reported in isolated renal mitochondria (71). The tendency toward cisplatin-driven reduction observed for PUFA phospholipid content (Fig. 5D) might also indirectly indicate lipid oxidation processes, which would be prevented by cilastatin. Interestingly, a number of PG species, including PG(34:1), the most abundant PG species in kidney, were increased in the medulla and cortex as a result of cisplatin treatment (58). Importantly, PG and CL are the few main lipid classes that show no recovery during cilastatin cotreatment in some cases, especially in the outer medulla (Fig. 2). There is clinical evidence of cisplatin-induced toxicity in the medullary loop of Henle (72). Considering that loop of Henle cells have a very high chloride concentration owing to cumulative transport through the Na^+:K^+:$2Cl^-$ pump, the cisplatin hydrolysis rate can be assumed to be considerably impaired, and, therefore, lower drug toxicity would be expected. For this reason, medullary accumulation of protein casts generally explains the clinical observations of damage in the loop of Henle (72). However, our finding of a reduction in mitochondrial CL,

which is especially visible in the medulla (mainly the loop of Henle and distal tubules), suggests direct cisplatin-induced mitochondrial damage via intrinsic apoptosis in the loop of Henle that is not fully reverted by cilastatin and that, for some species, remains unchanged.

Of note, most of the lipids that partially recovered after cotreatment with cilastatin and cisplatin were found in the medulla. Moreover, most of the few unrecovered lipids were also found in the medulla. These were mainly mitochondrial lipids (CL and PG) (Fig. 2), which could play an essential role in energy production, OS, and regulation of acute kidney injury. Our observations could be explained by direct cisplatin damage not protected by cilastatin that specifically inhibits renal DHP-I, which is located mainly in the cortex (66). However, most of the changes in lipid distribution in the cortex and medulla are secondary to cisplatin treatment, can be totally discerned with multivariate analysis (PCA and PLS-DA) (Fig. 6 and supplemental Figs. S3 and S4), and are fully or partially reversed with cilastatin. This finding could be extrapolated to any renal lesion mediated by Fas/Fas ligand. Consequently, cilastatin is an essential tool for differentiating between lipid changes caused by direct interaction with toxic drugs at any level and lipid changes secondary to a toxicity-driven insult in the proximal tubule. Although our data show that cisplatin-induced toxicity is mainly restricted to the cortical proximal tubule, changes in lipid distribution are huge and diverse, affecting the whole renal structure. Reversion of these changes by cilastatin exemplifies the enormous potential of this drug for improving renal function and diminishing structural changes.

The PCA/PLS-DA classification of the groups may be correlated with renal function and could be used as an alternative model for the assessment of nephrotoxicity and nephroprotection during therapy with cisplatin. This is clear when comparing merged lipid images from different groups with different distribution patterns. MSI enables hundreds of lipids to be monitored in a single analysis, and, considering the heterogeneous distribution of lipids in kidney, a plethora of possible combinations for visualizing kidney function status is available, with 31 lipid species showing totally recovered renal distribution compared with controls during protection from cisplatin-induced renal damage with cilastatin (Fig. 2).

In conclusion, MSI is presented as a powerful research tool for studying nephrotoxicity and kidney diseases in animal models and for the development of novel nephroprotective drugs, especially those targeting lipid rafts. MSI enables simultaneous understanding of complex processes, such as changes in mitochondrial structure and cell membrane phenomena related to apoptosis in acute kidney injury. Moreover, it provides straightforward information on the structural interconnection between the cortex and the medulla during renal damage and its recovery.

The authors thank José Manuel Lara for tissue sectioning and María Ángeles González-Nicolás for technical assistance with immunohistochemistry.

REFERENCES

1. Pabla, N., and Z. Dong. 2008. Cisplatin nephrotoxicity: mechanisms and renoprotective strategies. *Kidney Int.* **73:** 994–1007.
2. Kelland, L. 2007. The resurgence of platinum-based cancer chemotherapy. *Nat. Rev. Cancer.* **7:** 573–584.
3. Karasawa, T., and P. S. Steyger. 2015. An integrated view of cisplatin-induced nephrotoxicity and ototoxicity. *Toxicol. Lett.* **237:** 219–227.
4. Marullo, R., E. Werner, N. Degtyareva, B. Moore, G. Altavilla, S. S. Ramalingam, and P. W. Doetsch. 2013. Cisplatin induces a mitochondrial-ROS response that contributes to cytotoxicity depending on mitochondrial redox status and bioenergetic functions. *PLoS One.* **8:** e81162.
5. Messori, L., and A. Merlino. 2016. Cisplatin binding to proteins: a structural perspective. *Coord. Chem. Rev.* **315:** 67–89.
6. Jensen, M., M. Bjerring, N. C. Nielsen, and W. Nerdal. 2010. Cisplatin interaction with phosphatidylserine bilayer studied by solid-state NMR spectroscopy. *J. Biol. Inorg. Chem.*. **15:** 213–223.
7. Cepeda, V., M. A. Fuertes, J. Castilla, C. Alonso, C. Quevedo, and J. M. Perez. 2007. Biochemical mechanisms of cisplatin cytotoxicity. *Anticancer. Agents Med. Chem.* **7:** 3–18.
8. Miller, R. P., R. K. Tadagavadi, G. Ramesh, and W. B. Reeves. 2010. Mechanisms of cisplatin nephrotoxicity. *Toxins (Basel).* **2:** 2490–2518.
9. Moreno-Gordaliza, E., C. Giesen, A. Lazaro, D. Esteban-Fernandez, B. Humanes, B. Canas, U. Panne, A. Tejedor, N. Jakubowski, and M. M. Gomez-Gomez. 2011. Elemental bioimaging in kidney by LA-ICP-MS as a tool to study nephrotoxicity and renal protective strategies in cisplatin therapies. *Anal. Chem.* **83:** 7933–7940.
10. Humanes, B., A. Lazaro, S. Camano, E. Moreno-Gordaliza, J. A. Lazaro, M. Blanco-Codesido, J. M. Lara, A. Ortiz, M. M. Gomez-Gomez, P. Martin-Vasallo, et al. 2012. Cilastatin protects against cisplatin-induced nephrotoxicity without compromising its anticancer efficiency in rats. *Kidney Int.* **82:** 652–663.
11. Yang, Y., M. Song, Y. Liu, H. Liu, L. Sun, Y. Peng, F. Liu, M. A. Venkatachalam, and Z. Dong. 2016. Renoprotective approaches and strategies in acute kidney injury. *Pharmacol. Ther.* **163:** 58–73.
12. Camano, S., A. Lazaro, E. Moreno-Gordaliza, A. M. Torres, C. de Lucas, B. Humanes, J. A. Lazaro, M. M. Gomez-Gomez, L. Bosca, and A. Tejedor. 2010. Cilastatin attenuates cisplatin-induced proximal tubular cell damage. *J. Pharmacol. Exp. Ther.* **334:** 419–429.
13. Humanes, B., J. C. Jado, S. Camano, V. Lopez-Parra, A. M. Torres, L. A. Alvarez-Sala, E. Cercenado, A. Tejedor, and A. Lazaro. 2015. Protective effects of cilastatin against vancomycin-induced nephrotoxicity. *BioMed Res. Int.* **2015:** 704382.
14. Pérez, M., M. Castilla, A. M. Torres, J. A. Lázaro, E. Sarmiento, and A. Tejedor. 2004. Inhibition of brush border dipeptidase with cilastatin reduces toxic accumulation of cyclosporin A in kidney proximal tubule epithelial cells. *Nephrol. Dial. Transplant.* **19:** 2445–2455.
15. Humanes, B., S. Camaño, J. M. Lara, V. Sabbisetti, M. Á. González-Nicolás, J. V. Bonventre, A. Tejedor, and A. Lázaro. 2017. Cisplatin-induced renal inflammation is ameliorated by cilastatin nephroprotection. *Nephrol. Dial. Transplant.* **32:** 1645–1655.
16. Moreno-Gordaliza, E., D. Esteban-Fernandez, C. Giesen, K. Lehmann, A. Lazaro, A. Tejedor, C. Scheler, B. Canas, N. Jakubowski, M. W. Linscheid, et al. 2012. LA-ICP-MS and nHPLC-ESI-LTQ-FT-MS/MS for the analysis of cisplatin-protein complexes separated by two dimensional gel electrophoresis in biological samples. *J. Anal. At. Spectrom.* **27:** 1474–1483.
17. Esteban-Fernández, D., E. Moreno-Gordaliza, B. Cañas, M. A. Palacios, and M. M. Gómez-Gómez. 2010. Analytical methodologies for metallomics studies of antitumor Pt-containing drugs. *Metallomics.* **2:** 19–38.
18. Wilmes, A., C. Bielow, C. Ranninger, P. Bellwon, L. Aschauer, A. Limonciel, H. Chassaigne, T. Kristl, S. Aiche, C. G. Huber, et al. 2015. Mechanism of cisplatin proximal tubule toxicity revealed by integrating transcriptomics, proteomics, metabolomics and biokinetics. *Toxicol. In Vitro.* **30:** 117–127.
19. Perez, J. D., J. A. Colucci, M. M. Sakata, T. S. Cunha, D. Y. Arita, and D. E. Casarini. 2011. Proteomic approaches in understanding a detected relationship between chemotherapy-induced nephrotoxicity and cell respiration in HK-2 cells. *Nephron Physiol.* **119:** P1–P10.
20. Kwon, H. N., M. Kim, H. Wen, S. Kang, H-j. Yang, M-J. Choi, H. S. Lee, D. Choi, I. S. Park, Y. J. Suh, et al. 2011. Predicting idiopathic

toxicity of cisplatin by a pharmacometabonomic approach. *Kidney Int.* **79:** 529–537.
21. Portilla, D., S. Li, K. K. Nagothu, J. Megyesi, B. Kaissling, L. Schnackenberg, R. L. Safirstein, and R. D. Beger. 2006. Metabolomic study of cisplatin-induced nephrotoxicity. *Kidney Int.* **69:** 2194–2204.
22. Won, A. J., S. Kim, Y. G. Kim, K. B. Kim, W. S. Choi, S. Kacew, K. S. Kim, J. H. Jung, B. M. Lee, and H. S. Kim. 2016. Discovery of urinary metabolomic biomarkers for early detection of acute kidney injury. *Mol. Biosyst.* **12:** 133–144.
23. Zhao, Y-Y., N. D. Vaziri, and R-C. Lin. 2015. Lipidomics: new insight into kidney disease. *In* Advances in Clinical Chemistry. S. M. Gregory, editor. Elsevier, New York. 153–175.
24. Ognjanović, B. I., N. Z. Djordjević, M. M. Matić, J. M. Obradović, J. M. Mladenović, A. Š. Stajn, and Z. S. Saičić. 2012. Lipid peroxidative damage on cisplatin exposure and alterations in antioxidant defense system in rat kidneys: a possible protective effect of selenium. *Int. J. Mol. Sci.* **13:** 1790–1803.
25. Zhang, L., B. L. Peterson, and B. S. Cummings. 2005. The effect of inhibition of Ca2+-independent phospholipase A2 on chemotherapeutic-induced death and phospholipid profiles in renal cells. *Biochem. Pharmacol.* **70:** 1697–1706.
26. Naleskina, L. A., I. N. Todor, M. M. Nosko, N. Y. Lukianova, V. M. Pivnyuk, and V. F. Chekhun. 2013. Alteration in lipid composition of plasma membranes of sensitive and resistant Guerin carcinoma cells due to the action of free and liposomal form of cisplatin. *Exp. Oncol.* **35:** 192–197.
27. Yang, Y., J. Wang, L. Qin, Z. Shou, J. Zhao, H. Wang, Y. Chen, and J. Chen. 2007. Rapamycin prevents early steps of the development of diabetic nephropathy in rats. *Am. J. Nephrol.* **27:** 495–502.
28. Meistermann, H., J. L. Norris, H-R. Aerni, D. S. Cornett, A. Friedlein, A. R. Erskine, A. Augustin, M. C. De Vera Mudry, S. Ruepp, L. Suter, et al. 2006. Biomarker discovery by imaging mass spectrometry. *Mol. Cell. Proteomics.* **5:** 1876–1886.
29. Burnum, K. E., S. L. Frappier, and R. M. Caprioli. 2008. Matrix-assisted laser desorption/ionization imaging mass spectrometry for the investigation of proteins and peptides. *Annu. Rev. Anal. Chem. Palo Alto, Calif.*. **1:** 689–705.
30. Berry, K. A., J. A. Hankin, R. M. Barkley, J. M. Spraggins, R. M. Caprioli, and R. C. Murphy. 2011. MALDI Imaging of Lipid Biochemistry in Tissues by Mass Spectrometry. *Chem. Rev.* **111:** 6491–6512.
31. Jones, E. A., R. Shyti, R. J. M. van Zeijl, S. H. van Heiningen, M. D. Ferrari, A. M. Deelder, E. A. Tolner, A. M. J. M. van den Maagdenberg, and L. A. McDonnell. 2012. Imaging mass spectrometry to visualize biomolecule distributions in mouse brain tissue following hemispheric cortical spreading depression. *J. Proteomics.* **75:** 5027–5035.
32. Gode, D., and D. A. Volmer. 2013. Lipid imaging by mass spectrometry—a review. *Analyst.* **138:** 1289–1315.
33. Chughtai, K., and R. M. A. Heeren. 2010. Mass spectrometric imaging for biomedical tissue analysis. *Chem. Rev.* **110:** 3237–3277.
34. Spengler, B. 2015. Mass spectrometry imaging of biomolecular information. *Anal. Chem.* **87:** 64–82.
35. Römpp, A., S. Guenther, Z. Takats, and B. Spengler. 2011. Mass spectrometry imaging with high resolution in mass and space (HR2 MSI) for reliable investigation of drug compound distributions on the cellular level. *Anal. Bioanal. Chem.* **401:** 65–73.
36. Chumbley, C. W., M. L. Reyzer, J. L. Allen, G. A. Marriner, L. E. Via, C. E. Barry, and R. M. Caprioli. 2016. Absolute quantitative MALDI imaging mass spectrometry: a case of rifampicin in liver tissues. *Anal. Chem.* **88:** 2392–2398.
37. Muller, L., A. Kailas, S. N. Jackson, A. Roux, D. C. Barbacci, J. A. Schultz, C. D. Balaban, and A. S. Woods. 2015. Lipid imaging within the normal rat kidney using silver nanoparticles by matrix-assisted laser desorption/ionization mass spectrometry. *Kidney Int.* **88:** 186–192.
38. Marsching, C., M. Eckhardt, H-J. Gröne, R. Sandhoff, and C. Hopf. 2011. Imaging of complex sulfatides SM3 and SB1a in mouse kidney using MALDI-TOF/TOF mass spectrometry. *Anal. Bioanal. Chem.* **401:** 53–64.
39. Grove, K. J., P. A. Voziyan, J. M. Spraggins, S. Wang, P. Paueksakon, R. C. Harris, B. G. Hudson, and R. M. Caprioli. 2014. Diabetic nephropathy induces alterations in the glomerular and tubule lipid profiles. *J. Lipid Res.* **55:** 1375–1385.
40. Kaneko, Y., Y. Obata, T. Nishino, H. Kakeya, Y. Miyazaki, T. Hayasaka, M. Setou, A. Furusu, and S. Kohno. 2011. Imaging mass spectrometry analysis reveals an altered lipid distribution pattern in the tubular areas of hyper-IgA murine kidneys. *Exp. Mol. Pathol.* **91:** 614–621.
41. Ruh, H., T. Salonikios, J. Fuchser, M. Schwartz, C. Sticht, C. Hochheim, B. Wirnitzer, N. Gretz, and C. Hopf. 2013. MALDI imaging MS reveals candidate lipid markers of polycystic kidney disease. *J. Lipid Res.* **54:** 2785–2794.
42. Moreno-Gordaliza, E., D. Esteban-Fernández, A. Lázaro, B. Humanes, S. Aboulmagd, A. Tejedor, M. W. Linscheid, and M. M. Gómez-Gómez. 2017. MALDI-LTQ-Orbitrap mass spectrometry imaging for lipidomic analysis in kidney under cisplatin chemotherapy. *Talanta.* **164:** 16–26.
43. Gallego-Delgado, J., A. Lazaro, D. Gomez-Garre, J. I. Osende, M. L. Gonzalez-Rubio, M. Herraiz, F. Manzarbeitia, J. Fortes, A. Fernandez-Cruz, and J. Egido. 2006. Long-term organ protection by doxazosin and/or quinapril as antihypertensive therapy. *J. Nephrol.* **19:** 588–598.
44. Schramm, T., A. Hester, I. Klinkert, J-P. Both, R. M. A. Heeren, A. Brunelle, O. Laprévote, N. Desbenoit, M-F. Robbe, M. Stoeckli, et al. 2012. imzML—a common data format for the flexible exchange and processing of mass spectrometry imaging data. *J. Proteomics.* **75:** 5106–5110.
45. Robichaud, G., K. P. Garrard, J. A. Barry, and D. C. Muddiman. 2013. MSiReader: an open-source interface to view and analyze high resolving power MS imaging files on Matlab platform. *J. Am. Soc. Mass Spectrom.* **24:** 718–721.
46. Fahy, E., D. Cotter, M. Sud, and S. Subramaniam. 2011. Lipid classification, structures and tools. *Biochim. Biophys. Acta.* **1811:** 637–647.
47. Kind, T., K-H. Liu, D. Y. Lee, B. DeFelice, J. K. Meissen, and O. Fiehn. 2013. LipidBlast in silico tandem mass spectrometry database for lipid identification. *Nat. Methods.* **10:** 755–758.
48. Xia, J., I. V. Sinelnikov, B. Han, and D. S. Wishart. 2015. MetaboAnalyst 3.0—making metabolomics more meaningful. *Nucleic Acids Res.* **43:** W251–W257.
49. Han, W. K., V. Bailly, R. Abichandani, R. Thadhani, and J. V. Bonventre. 2002. Kidney Injury Molecule-1 (KIM-1): a novel biomarker for human renal proximal tubule injury. *Kidney Int.* **62:** 237–244.
50. Shoeb, M., N. H. Ansari, S. K. Srivastava, and K. V. Ramana. 2014. 4-hydroxynonenal in the pathogenesis and progression of human diseases. *Curr. Med. Chem.* **21:** 230–237.
51. Yao, X., K. Panichpisal, N. Kurtzman, and K. Nugent. 2007. Cisplatin nephrotoxicity: a review. *Am. J. Med. Sci.* **334**: 115–124.
52. Tejedor, A., A. M. Torres, M. Castilla, J. A. Lazaro, C. de Lucas, and C. Caramelo. 2007. Cilastatin protection against cyclosporin A-induced nephrotoxicity: clinical evidence. *Curr. Med. Res. Opin.* **23:** 505–513.
53. Birnbaum, J., F. M. Kahan, H. Kropp, and J. S. Macdonald. 1985. Carbapenems, a new class of beta-lactam antibiotics: discovery and development of imipenem/cilastatin. *Am. J. Med.* **78:** 3–21.
54. Nematbakhsh, M., and H. Nasri. 2013. Cisplatin nephrotoxicity may be sex related. *Kidney Int.* **83:** 1201.
55. Stillwell, W. 2016. Membrane polar lipids. *In* An Introduction to Biological Membranes. 2nd edition. Elsevier, New York. 63–87.
56. D'Souza, K., and R. M. Epand. 2014. Enrichment of phosphatidylinositols with specific acyl chains. *Biochim. Biophys. Acta.* **1838:** 1501–1508.
57. Balsinde, J., M. V. Winstead, and E. A. Dennis. 2002. Phospholipase A2 regulation of arachidonic acid mobilization. *FEBS Lett.* **531:** 2–6.
58. Choi, J., T. Yin, K. Shinozaki, J. W. Lampe, J. F. Stevens, L. B. Becker, and J. Kim. 2018. Comprehensive analysis of phospholipids in the brain, heart, kidney, and liver: brain phospholipids are least enriched with polyunsaturated fatty acids. *Mol. Cell. Biochem.* **442:** 187–201.
59. Schütze, S., T. Machleidt, and M. Krönke. 1992. Mechanisms of tumor necrosis factor action. *Semin. Oncol.* **19:** 16–24.
60. Schlondorff, D., and R. Ardaillou. 1986. Prostaglandins and other arachidonic acid metabolites in the kidney. *Kidney Int.* **29:** 108–119.
61. Meyer zu Heringdorf, D., and K. H. Jakobs. 2007. Lysophospholipid receptors: signalling, pharmacology and regulation by lysophospholipid metabolism. *Biochim. Biophys. Acta.* **1768:** 923–940.
62. Mariño, G., and G. Kroemer. 2013. Mechanisms of apoptotic phosphatidylserine exposure. *Cell Res.* **23:** 1247–1248.
63. Hoffmann, P. R., A. M. deCathelineau, C. A. Ogden, Y. Leverrier, D. L. Bratton, D. L. Daleke, A. J. Ridley, V. A. Fadok, and P. M.

Henson. 2001. Phosphatidylserine (PS) induces PS receptor-mediated macropinocytosis and promotes clearance of apoptotic cells. *J. Cell Biol.* **155:** 649–659.
64. Vance, J. E., and G. Tasseva. 2013. Formation and function of phosphatidylserine and phosphatidylethanolamine in mammalian cells. *Biochim. Biophys. Acta.* **1831:** 543–554.
65. Schenkel, L. C., and M. Bakovic. 2014. Formation and regulation of mitochondrial membranes. *Int. J. Cell Biol.* **2014:** 709828.
66. Kriz, W., and M. Elger. 2010. Renal anatomy. *In* Comprehensive Clinical Nephrology. 4th edition. J. Floege, R. J. Johnson, and J. Feehally, editors. Mosby, Philadelphia. 3–14.
67. Osman, C., D. R. Voelker, and T. Langer. 2011. Making heads or tails of phospholipids in mitochondria. *J. Cell Biol.* **192:** 7–16.
68. Tyurina, Y. Y., S. M. Poloyac, V. A. Tyurin, A. A. Kapralov, J. Jiang, T. S. Anthonymuthu, V. I. Kapralova, A. S. Vikulina, M-Y. Jung, M. W. Epperly, et al. 2014. A mitochondrial pathway for biosynthesis of lipid mediators. *Nat. Chem.* **6:** 542–552.
69. Crimi, M., and M. D. Esposti. 2011. Apoptosis-induced changes in mitochondrial lipids. *Biochim. Biophys. Acta.* **1813:** 551–557.
70. Wang, H-Y. J., S. N. Jackson, and A. S. Woods. 2007. Direct MALDI-MS analysis of cardiolipin from rat organs sections. *J. Am. Soc. Mass Spectrom.* **18:** 567–577.
71. Santos, N. A. G., C. S. Catão, N. M. Martins, C. Curti, M. L. P. Bianchi, and A. C. Santos. 2007. Cisplatin-induced nephrotoxicity is associated with oxidative stress, redox state unbalance, impairment of energetic metabolism and apoptosis in rat kidney mitochondria. *Arch. Toxicol.* **81:** 495–504.
72. Safirstein, R., J. Winston, M. Goldstein, D. Moel, S. Dikman, and J. Guttenplan. 1986. Cisplatin nephrotoxicity. *Am. J. Kidney Dis.* **8:** 356–367.